RSC Advances

ROYAL SOCIETY OF CHEMISTRY

www.rsc.org/advances

Cite this: DOI: 10.1039/c0xx00000x

www.rsc.org/xxxxxx

PAPER

Solvothermal synthesis of β-tricalcium phosphate porous nanospheres by using organic phosphorus source and their biomedical potentials

Genxing Zhu,[a] Yadong Hu,[ab] Yuling Yang,[a] Ruibo Zhao,[a] and Ruikang Tang*[ab]

Received (in XXX, XXX) Xth XXXXXXXXX 20XX, Accepted Xth XXXXXXXXX 20XX

DOI: 10.1039/b000000x

β-tricalcium phosphate (TCP) is an important biomedical material but the synthesis of β-TCP with uniform nanostructure still remains a challenge. We report that β-TCP porous nanospheres could be prepared feasibly by a solvothermal method, in which trimethyl phosphate was used as the organic phosphorus source. The as-prepared 120 nm nanospheres were assembled by 15-25 nm nano building blocks with a multilevel structure, resulting in multiple pore size distributions. As a result, they have excellent cytocompatibility, high drug loading and protein adsorption capacities, and sustained release behaviours. It follows that the uniform porous β-TCP nanospheres are more promising for applications in biomedical fields.

Introduction

Calcium phosphate (CaP) materials are the ideal biomaterials due to their excellent biocompatibility, which have the promising applications in drug and gene delivery,[1-6] tissue engineering[7-10] and non-medical industry applications.[11-16] Among the various kinds of CaP, β-tricalcium phosphate (TCP: $Ca_3(PO_4)_2$) has received more attentions due to its good tissue compatibility, fast bone regeneration and resorbability,[17-19] which has been developed as an important biomaterial for bone and dental repair.[20-25] However, the physicochemical properties of synthetic CaP including β-TCP strongly depend upon the crystallite size and morphology. Up to now, the crystallization control is still a great challenge for β-TCP synthesis. Analogous to the other CaP phases, β-TCP is a sparingly soluble electrolyte. Generally, a relatively high supersaturation is always required to ensure its spontaneous crystallization, which was unfavourable for the size and morphology regulations. In the past decades, various methods such as sol–gel technique,[26-29] microwave assisted method,[30] combustion or flame synthesis[31, 32] and precursor transformation[33] have been reported to improve β-TCP synthesis. But the resulted materials always have the poor size distribution with irregular morphology, which make them difficult for strict biomedical evaluation.

In order to prepare uniform β-TCP crystallites, the significant reduction of the critical supersaturation is of importance. Different from inorganic phosphate, organic phosphorus compound generally requires certain condition to hydrolyze for the release of free phosphate ions, which can be used to avoid the fast nucleation and disordered growth. Herein, we report a new synthetic strategy of β-TCP by using a solvothermal method with trimethyl phosphate. The as-prepared β-TCP nanospheres have uniform moprhology and size distribution. More importantly, they have a multiple level pore size distribution, which benefit drug delivery and protein adsorption.

Results and Discussion

The strategy for the solvothermal synthesis of β-TCP porous nanospheres is illustrated in Scheme 1. Trimethyl phosphate molecules hydrolyze to produce PO_4^{3-} ions under solvothermal condition. PO_4^{3-} ions then react with Ca^{2+} ions to form15-25 nm β-TCP nanoparticles, and these nanoparticles further assembled into uniform β-TCP porous nanospheres with a size of 120 nm.

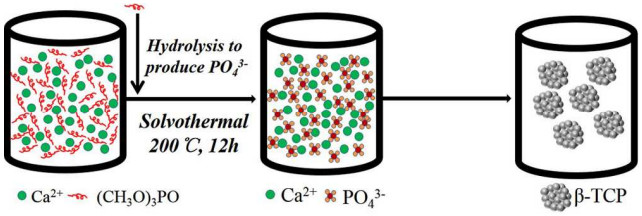

Scheme 1. Schematic illustration of the strategy for the fabrication of β-TCP porous nanospheres by using $(CH_3O)_3PO$ as an organic phosphorus source by a solvothermal method.

The resulted material was observed by scanning electron microscopy (SEM) and transmission electron microscopy (TEM). As shown in Figure 1a, the spheres had a relatively uniform size in the solid state and the diameters were about 100-130 nm. Dynamic light scattering (DLS) size distribution (Figure 1d) confirmed that in the solution state, most particles located within a narrow size distribution range of 120 ± 30 nm. It should be noted that the spheres had rough surface and substructure. Under high-resolution TEM, the nanospheres consisted of 15 - 25 nm nanoparticles as building blocks, which were assembled into the porous structure. The crystal phase was characterized by X-ray powder diffraction (XRD, Figure 1e) and the pattern could be indexed to a single phase of well-crystallized β-TCP (JCPDS 09-0169). Figure 1f shows the Fourier transform infrared (FTIR)

Cite this: DOI: 10.1039/c0xx00000x

www.rsc.org/xxxxxx

PAPER

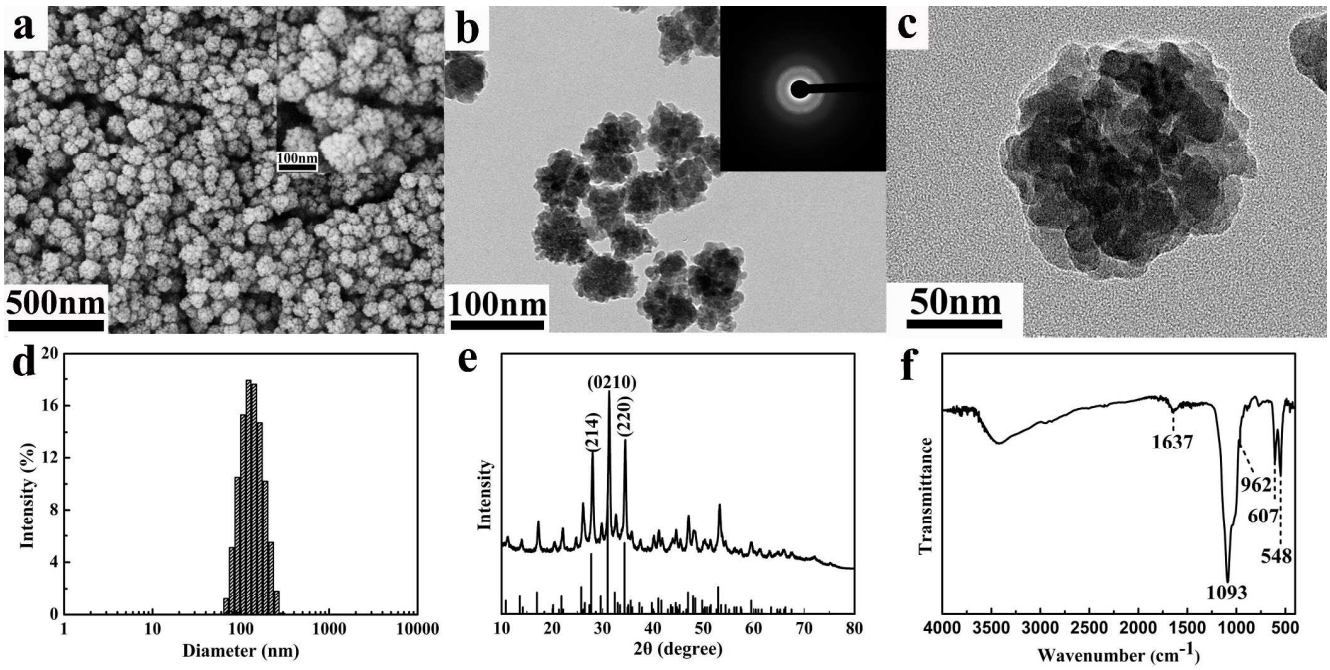

Figure 1. Characterization of the as-prepared β-TCP porous nanospheres. (a) SEM image; insert the magnified mage, which shows more details about the porous structure and rough surface. (b) TEM image; insert is the corresponding SAED pattern. (c) HRTEM image. (d) Dynamic light scattering (DLS) size distribution in water. (e) XRD pattern and (f) FTIR spectra.

spectra of the material. The broad peak at around 3470 cm^{-1} was assigned to adsorbed water and the band at 1637 cm^{-1}, the ν_2 bending mode of water molecules. The characteristic bands of PO_4^{3-} ions located at about 1093, 1033, 962, 607 and 548 cm^{-1}. Of these absorption peaks, the bands at 1093 and 1033 cm^{-1} were assigned to the ν_3 vibrations of the P-O bond of PO_4^{3-}. The peak at 962 cm^{-1} was due to the ν_1 stretching mode of the P-O bond of PO_4^{3-}. The peaks at 607 and 548 cm^{-1} referred to the ν_4 bending mode of O-P-O bonds. These results were consistent with the XRD analysis and those previously reported.[29, 30, 34] Moreover, there was no obvious peak originated from the organic phosphorus source. It implied the minimal amount of organic residue in the β-TCP nanospheres.

The morphologies of the samples prepared under different conditions were also examined. We found that solid phase was sensitive to the solvent phase. For example, hydroxyapatite (HAP) rather than β-TCP was formed if DMF-water binary or DMF-water-EG ternary solvents was used as the reaction medium (Figure S1 and S2). Besides, the amounts of β-TCP obtained could be increased by increasing the solvothermal temperature or the reaction time but the morphology and size were not affected.

N_2 adsorption–desorption was performed to analyze the porous structure of the β-TCP. As shown in Figure 2, at a lower relative pressure range (P/P_0 > 0.5), the hysteresis loop was clearly observed, indicating the presence of mesopores. Moreover, the adsorption did not reach saturation and the capacity increased

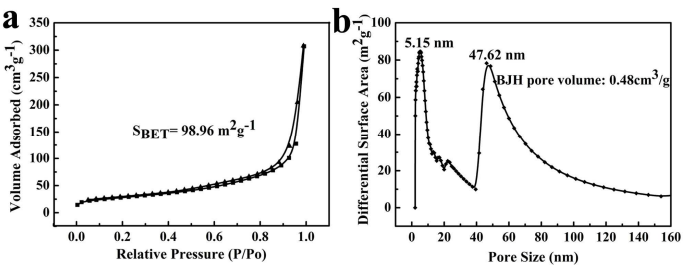

Figure 2. N_2 adsorption–desorption isotherm (a) and pore size distribution (b) of the as-prepared β-TCP porous nanospheres.

quickly at a relatively high pressure range (P/P_0 > 0.9), which meant the presence of larger interparticles mesopores and macropores. Therefore, the nanospheres had a multiple level pore size distribution (a sharp band centered at pore size of 5.15 nm and a relatively broad band centered at pore size of 47.62 nm), manifesting their porous characteristics. The mesopores were ascribed to the texture porosity formed by β-TCP nanoparticles aggregation and the macropores were arisen from the interspace among the nanospheres. The Brunauer–Emmett–Teller (BET) specific surface area and the Barrett–Joyner–Halenda (BJH) desorption cumulative pore volume of the as-prepared β-TCP porous nanospheres were about 98.96 m^2/g and 0.48 cm^3/g, respectively. The porosity of the nanospheres based on the BJH

method was consistent with that observed by SEM and TEM. The relatively large specific surface area and pore volume of the β-TCP nanospheres would be favourable for their applications in drug delivery and protein adsorption.

The cytotoxicity tests of the β-TCP porous nanospheres were performed using human cervical carcinoma HeLa cells. The MTT assay showed no appreciable toxicity when the cells were co-cultured with the material at concentrations of 0.1~500 μg/mL (Figure 3). Actually, the β-TCP nanospheres could even facilitate the cell proliferation. This high cytocompatibility could be explained by the chemical nature of the porous nanospheres, which would biomimic the inorganic phase in the hard tissues.[35]

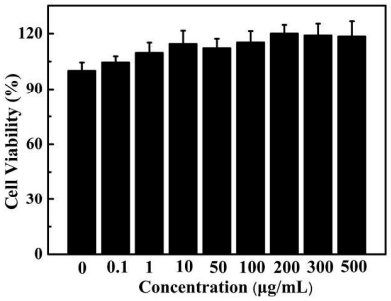

Figure 3. Cytotoxicity tests of the as-prepared β-TCP porous nanospheres.

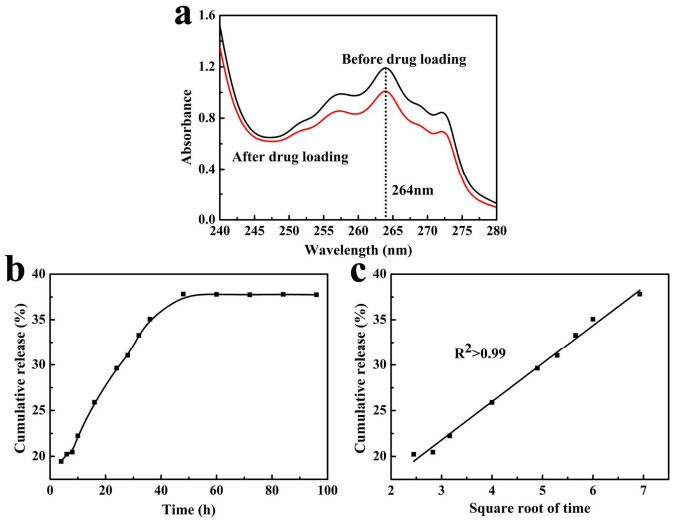

Figure 4. (a) UV-vis absorption spectra of the hexane solution containing ibuprofen before and after ibuprofen loading in the as-prepared β-TCP porous nanospheres. Each solution was diluted 50 times; (b) ibuprofen drug-release curve in PBS solution (pH=7.4) of the ibuprofen-loaded β-TCP porous nanospheres; (c) the cumulative drug-release percentage as a function of the square root of the release time.

We investigated the drug-loading and -release performances of the β-TCP porous nanospheres. Ibuprofen (IBU), a typical anti-inflammatory drug, was chosen as the model drug. Figure 4a shows the UV-vis absorption spectra of the hexane solution containing ibuprofen before and after the drug loading. The absorption spectra of ibuprofen in hexane solution had a characteristic absorption peak of ibuprofen at 264 nm and the β-TCP porous nanospheres exhibited a good drug-loading performance (33.16 mg drug per gram carrier).

Figure 4b shows the drug-release behaviour of the β-TCP porous nanosphere drug-delivery system in PBS solution (pH=7.4). The β-TCP porous nanosphere drug-delivery system exhibited a slow and sustained release of ibuprofen in a period of about 50 h and reached a plateau at about 37.5%, which might be due to the relatively strong interaction between ibuprofen molecules and β-TCP. Figure 4c shows the relationship between the cumulative amount of the released drug and the square root of release time for the β-TCP porous nanosphere drug-delivery system, which had a good linear relationship with a high regression coefficient of >0.99. This indicated that the drug release of the β-TCP porous nanosphere drug delivery system was governed by a diffusion process, which was consistent with the established Higuchi model.[36, 37]

We also investigated the protein adsorption and release performance of the β-TCP porous nanospheres using hemoglobin (Hb) as a model protein. The adsorption of Hb onto the surface of the nanospheres was confirmed by FTIR spectroscopy (Figure 5a). By comparing the FTIR spectra of the nanospheres before and after the Hb-protein adsorption with that of pure Hb, we could see that two obvious amide peaks (at about 1655 and 1558 cm^{-1}) appeared for the nanospheres after the protein adsorption, which originated from Hb. This result indicated that the Hb molecules were loaded into the β-TCP. The adsorption of Hb on the nanospheres was also investigated at different initial concentrations of Hb. As shown in Figure 5b, the amount of adsorbed Hb on the as-prepared β-TCP porous nanospheres increased with increasing initial concentration of Hb in the range of 0~3 mg/mL. Compared with some previous reports of the CaP materials,[38, 39, 40] the significant increase in Hb adsorption on our β-TCP porous nanospheres could be understood by their relatively large BET specific surface area and BJH desorption cumulative pore volume.

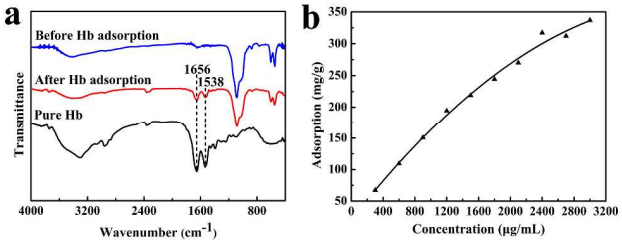

Figure 5. (a) FTIR spectra of pure Hb protein, the as-prepared β-TCP porous nanospheres before and after Hb-protein adsorption; (b) Hb-protein adsorption curve at different initial concentrations of Hb by the as-prepared β-TCP porous nanospheres.

Langmuir,[41, 42] Freundlich[43] and Temkin[44] isotherm models were employed to investigate the Hb adsorption process. Langmuir isotherm model has been successfully applied to many adsorption processes. It assumes that adsorption occurs at specific homogenous sites within the adsorbent. Once a molecule

occupies a site, no further adsorption will take place at the site. The linear form of the Langmuir isotherm equation can be represented by the following equation:

$$\frac{c_e}{q_e} = \frac{c_e}{q_m} + \frac{1}{q_m b} \quad (1)$$

where q_e (mg/g) is the amount of adsorbate that is adsorbed at equilibrium, c_e (μg/mL), the equilibrium concentration of adsorbate in the solution, q_m (mg/g), the maximum adsorption capacity that corresponds to complete monolayer coverage, and b, the equilibrium constant (mL/μg).

The Freundlich isotherm assumes a heterogeneous system with different energies of active sites and reversible adsorption, which is not restricted to monolayer sorption. It is an empirical equation which is used for the description of multilayer adsorption with interaction between adsorbed molecules. The Freundlich isotherm is shown as below:

$$q_e = kc_e^{1/n} \quad (2)$$

where k (mg/g) is Freundlich constant representing the adsorption capacity, n (dimensionless), an empirical parameter related to the adsorption intensity. The value of *n* varies with the heterogeneity of the adsorbent and for favourable adsorption process the value of n should lie in the range of 1-10.

Temkin isotherm assumes that the heat of adsorption of all the molecules in the layer would decrease linearly with coverage and the adsorption is characterized by a uniform distribution of binding energies, up to some maximum binding energy. The Temkin isotherm equation is as follow:

$$q_e = \frac{RT}{b} \ln(A_T c_e) \quad (3)$$

where R is the gas constant (8.314 J mol^{-1} K^{-1}), T, the absolute temperature, A_T (L/mg), the Temkin equilibrium binding constant and b (dimensionless), the Temkin isotherm constant.

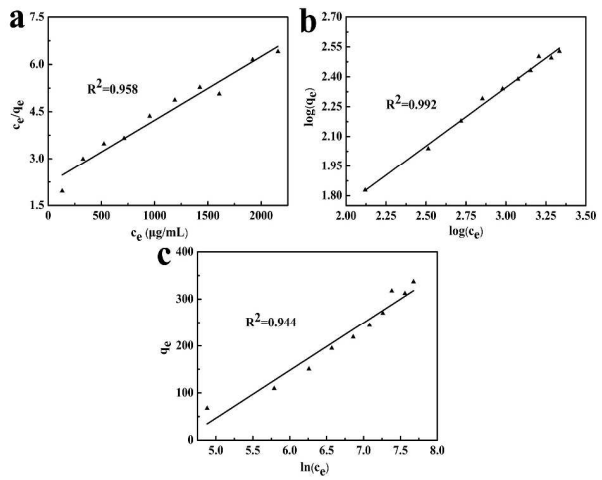

Figure 6. The fitting of different adsorption isotherms for Hb adsorption onto the as-prepared β-TCP nanospheres. (a) Langmuir isotherm model, (b) Freundlich isotherm model, (c) Temkin isotherm model.

The fitting of different adsorption isotherms for Hb adsorption onto the β-TCP porous nanospheres are shown in Figure 6. The regression coefficient R^2 obtained from the Freundlich model is much higher than those from the Langmuir model and Temkin model, suggesting that the Freundlich isotherm fits better with the experimental data. It can be attributed to the heterogeneous distribution of active sites on the β-TCP porous nanospheres surface, which is consistent with the texture porosity observed by SEM and TEM. Moreover, the Freundlich constant n is found to be 1.69 ($10 > n > 1$), which indicates that the adsorption of Hb on the porous nanospheres is a favourable process.

The adsorption kinetics of Hb on the β-TCP porous nanospheres is shown in Figure 7. The Lagergren pseudo-first order,[45] pseudo-second order[46] and intra-particle diffusion[47] kinetic models have been used to examine experimental data.

The Lagergren pseudo-first-order equation is expressed as:

$$\ln(q_e - q_t) = \ln(q_e) - k_1 t \quad (4)$$

where q_e and q_t are the amount of adsorbate adsorbed (mg/g) at equilibrium and at time t, respectively. t is the contact time (min) and k_1, the rate constant (min^{-1}). The values of $k_1$and q_e were calculated from the plot of $ln(q_e - q_t)$ versus t.

The pseudo-second order model, proposed by Ho and McKay, can be represented in the following linear form:

$$\frac{t}{q_t} = \frac{t}{q_e} + \frac{1}{k_2 q_e^2} \quad (5)$$

where $k_2 q_e^2$ is the initial adsorption rate (mg/g), k_2, the pseudo-second-order rate constant (g mg^{-1} min^{-1}). The values of q_e and k_2 were obtained by a linear plot t/qt versus t.

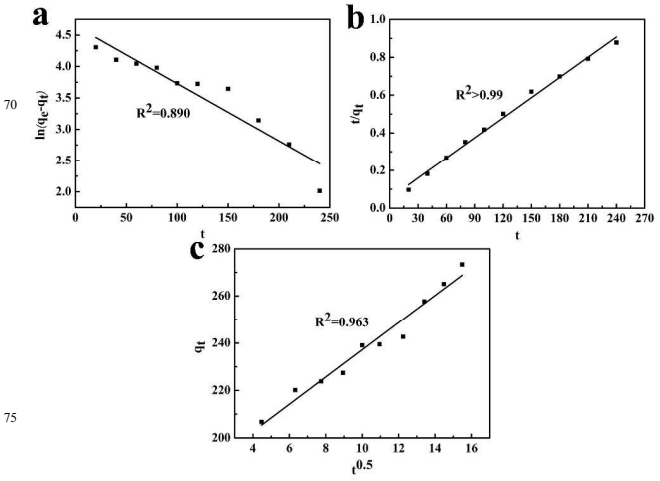

Figure 7. The fitting of different kinetic models for Hb adsorption onto the as-prepared β-TCP porous nanospheres. (a) Lagergren pseudo-first order, (b) Pseudo-second order, (c) Intra-particle diffusion.

The intraparticle diffusion equation can be written as:

$$q_t = k_{intra} t^{0.5} + C \quad (6)$$

where C represents the intercept (mg/g) and k_{intra} is the intraparticle diffusion rate constant (mg g^{-1} $min^{-0.5}$). A plot of q_t versus $t^{0.5}$ should be in straight line if the adsorption process follows the intraparticle diffusion; meanwhile if the line passes through the origin then intra particle diffusion will be the sole controlling step.

As shown in Figure 7, it can be found that the regression coefficient R^2 obtained from the pseudo-second order model is much higher than those from other models, suggesting that the pseudo-second order model fits better with the experimental data.

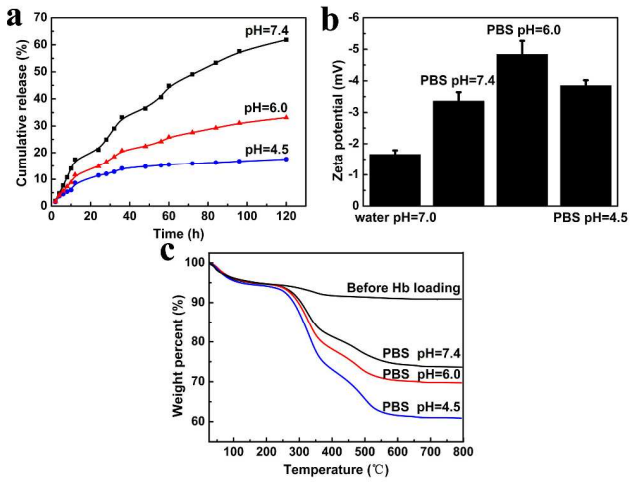

Figure 8. (a) Cumulative Hb release from Hb-loaded β-TCP porous nanospheres at different pH values of 4.5, 6.0 and 7.4 in PBS at 37 °C; (b) Zeta potentials of the as-prepared β-TCP porous nanospheres in different solvents at different pH; (c) TGA curves of the as-prepared β-TCP porous nanospheres before and after Hb adsorption in PBS solution at different pH values.

The Hb release behaviours were investigated in phosphate buffered saline (PBS) with different pH values of 4.5, 6.0 and 7.4, and the Hb cumulative release curves are shown in Figure 8a. We can see that the release of Hb in PBS solution was dependent on the pH value and the protein adsorption system exhibited a slow and sustained Hb release over a period of 120 h. The amount of Hb that was released from the β-TCP porous nanospheres in PBS at pH 7.4 was much higher than that at pH 6.0 and pH 4.5. The release rate decreased in the following order: pH 7.4 > pH 6.0 > pH 4.5. The cumulative amount of released Hb reached 61.9% at pH 7.4, 33.1% at pH 6.0, and 17.6% at pH 4.5 after 120 h. This result might be explained by the electrostatic interactions between Hb molecules and the β-TCP porous nanospheres, which would be discussed further on the basis of zeta potentials. In general, protein adsorption is attributed to van der Waals, electrostatic, and hydrophobic interactions.[48] The isoelectric point (pI) of Hb is within the range 6.8-7.0.[49] When the pH value of the PBS solution is higher than the pI value of Hb, the Hb molecules become negatively charged, whereas, when the pH value is below the pI value, the Hb molecules become positively charged. As shown in Figure 8b, the β-TCP porous nanospheres were all negatively charged in PBS solution at pH 7.4, 6.0, and 4.5. Thus, when the pH value of the PBS solution was 7.4, both the Hb molecules and the β-TCP porous nanospheres were negatively charged and the electrostatic repulsion effect accelerated the release of Hb from the β-TCP. When the pH values were 6.0 and 4.5, the Hb molecules became positively charged and the electrostatic attraction effect restrained the release of Hb, and the lower the pH value, the stronger the electrostatic interactions and the slower the release of Hb.

To further verify the above analysis, we investigated the amount of Hb that was adsorbed onto the β-TCP porous nanospheres in PBS solution at different pH values at a concentration of 3 mg/mL. As shown in Figure 8c, the amount of adsorbed Hb on the β-TCP porous nanospheres increased with decreasing pH value. This result could be explained by the electrostatic interactions between the Hb molecules and the β-TCP porous nanospheres. The lower the pH value of the PBS solution, the stronger the electrostatic attraction effect led to more Hb adsorbed onto the β-TCP porous nanospheres. This result was consistent with the above Hb-release behaviours in PBS solution at different pH values.

Conclusion

A new solvothermal strategy for the synthesis of β-TCP porous nanospheres with trimethyl phosphate as an organic phosphorus source has been demonstrated. The as-prepared β-TCP nanospheres (average diameter about 120nm) were composed of 15~25nm β-TCP nanoparticles, which were assembled into nanostructured porous nanospheres. They have a multiple level pore size distribution with the specific surface area of 98.96 m^2/g. These β-TCP porous nanospheres are explored for potential applications in drug delivery and protein adsorption and release. The experimental results indicate that they have excellent cytocompatibility and a relatively high drug loading capacity and high protein adsorption ability, and sustained drug and protein release. Moreover, Freundlich isotherm and pseudo-second order models fit better with the Hb adsorption data. Thus, the as-prepared β-TCP porous nanospheres are promising for applications in biomedical fields, such as drug delivery and protein adsorption

Experimental section

Preparation of β-TCP porous nanospheres: All the chemicals used in the sample preparation were used as received without further purification. In a typical synthesis of the β-TCP porous nanospheres, 0.2664 g $CaCl_2$ was dissolved in 60 mL mixed solvents of ethylene glycol (EG) and N, N-dimethylformamide (DMF) with volume ratio of 1 : 1 under magnetic stirring at room temperature to form a clear solution. Then 0.570 mL trimethyl phosphate was added to the former solution with continually magnetic stirring to form a homogeneous solution. After stirring for 15 min, the resulting solution was transferred to a Teflon autoclave, sealed and heated to 200 °C and maintained at this temperature for 12 h. After cooling to room temperature, the product was separated by centrifugation, washed with deionized water and ethanol several times, and then dried in vacuum at 30 °C for 48 h.

Characterization: The as-prepared samples were characterized using X-ray powder diffraction (XRD) (Rigaku Dmax 2200, Cu-Kα radiation, λ=1.5416 Å), scanning electron microscopy (FE-SEM, Hitachi, S-4800), high resolution transmission electron microscopy (HRTEM, JEOL JEM 2100F), transmission electron microscopy (TEM, Hitachi, HT-7700), Fourier transform infrared (FTIR) (IRAffinity-1, Shimadzu), Brunauer–Emmett–Teller (BET) surface area (ASAP 2020 M, Micromeritics), and thermogravimetric (TG) analysis (SDT Q600, heating rate 10 °C min^{-1}, air atmosphere). The ibuprofen and hemoglobin (Hb) concentrations were analyzed using a UV-vis spectrophotometer (T60, Pg instruments) at wavelengths of 264 nm and 405 nm, respectively. The Zeta potential values were measured using a Zetasizer Nano S analyzer (Malvern).

In vitro cytotoxicity tests: Human cervical carcinoma HeLa cells were seeded in a 96-well plate at approximately 1×10^4 cells per well and cultured in Dulbecco's modified Eagle's medium (DMEM, Gibco) supplemented with 10 % heat-inactivated fetal bovine serum (FBS) at 37 °C in a 5 % CO_2 incubator. Then, supernatant of each well was drawn off carefully and 100 μL serial β-TCP with indicated concentrations in DMEM containing 10% FBS were added into the wells, and DMEM containing 10% FBS was used as control, respectively. 20 μL MTT was added into each well after 24 h, then, the cells were incubated at 37 °C for another 4 h and 200 μL lysis solution (10% Sodium dodecyl sulfate, 5% Isobutanol, 0.012mol/L HCl) was added into each well and incubated at 37 °C overnight. Finally, the optical density at 570 nm (absorption value) was measured by a BioTek Eon monochromator-based multifunction microplate reader. The data was representative as the mean value of six parallel experiments.

Drug loading and in vitro drug release: Typical drug-loading and in vitro drug-release experiments were performed as follows: 200 mg β-TCP porous nanospheres were added into 20 mL hexane solution with an ibuprofen concentration of 40 mg/mL. The resulting suspension was continuously shaken in a sealed vessel at 37 °C for 24 h, followed by centrifugation and drying in vacuum to obtain the drug-loaded β-TCP nanospheres. For the drug-release assay, the drug-loaded β-TCP nanospheres (40 mg) were immersed in phosphate buffered saline (PBS, 8 mL, pH 7.4) at 37 °C with constant shaking (140 rpm). The shaking device was a desk-type constant-temperature oscillator (HZ-8811K, China). The drug release medium (0.4 mL) was withdrawn for analysis by UV-vis absorption spectroscopy at a wavelength of 264 nm at given time intervals and replaced with the same volume of fresh preheated PBS solution (37 °C).

In vitro protein adsorption: Hemoglobin (Hb) was chosen as a model protein for our investigation. The protein adsorption experiments at different protein concentrations were performed as follows: 5 mg β-TCP porous nanospheres were immersed in aqueous solutions containing variable protein concentrations (2 mL, 0-3 mg/mL). Each solution was shaken at a constant rate (140 rpm) for 4 h at 37 °C. Then, the solution was centrifuged and the amount of protein in the supernatant was measured by UV-vis absorption analysis at a wavelength of 405 nm. The protein adsorption experiments at different pH values were performed as follows: 80 mg β-TCP porous nanospheres were immersed in a solution of Hb in PBS solution (3 mg/mL, 20 mL) at different pH values (pH 7.4, 6.0 and 4.5). Each solution was shaken at a constant rate (140 rpm) for 4 h at 37 °C. Then, the solution was centrifuged and the β-TCP porous nanospheres were dried in vacuum at 30 °C. The amounts of protein that was adsorbed on the β-TCP nanospheres at different pH values were measured by TGA.

In vitro protein release: For the in vitro protein release from β-TCP nanospheres, 80 mg β-TCP porous nanospheres were immersed in 8 mL hemoglobin (Hb) aqueous solution with a concentration of 3 mg/mL, and the solution was shaken at a constant rate for 4 h at 37 °C, followed by centrifugation and drying in vacuum to obtain the protein-adsorbed β-TCP porous nanospheres. The in vitro protein-release experiments at different pH values were performed as follows: The powdered Hb-loaded β-TCP nanospheres (8 mg) were immersed in PBS solution (8 mL) at different pH values (pH 7.4, 6.0 and 4.5) at 37 °C with constant shaking (140 rpm). The protein-release solution (0.4 mL) was withdrawn for UV-vis absorption analysis at given time intervals and replaced with the same volume and the same pH value of fresh PBS (37 °C, pH 7.4, 6.0 and 4.5).

Acknowledgements

We thank Qiaohong He and Fang Chen for their assistances in material characterizations. This work was supported by the Fundamental Research Funds for the Central Universities and the National Natural Science Foundation of China (No. 91127003).

Notes and references

[a] *Center for Biomaterials and Biopathways, Department of Chemistry, Zhejiang University, Hangzhou, China. Fax: (+)86 571 87953736; Tel: (+)86 571 87953736; E-mail: rtang@zju.edu.cn*
[b] *Qiushi Academy for Advanced Studies, Zhejiang University, Hangzhou, China.*

1. M.-P. Ginebra, C. Canal, M. Espanol, D. Pastorino, E. B. Montufar, *Adv. Drug Deliver. Rev* 2012, **64**, 1090-1110.
2. E. Verron, I. Khairoun, J. Guicheux, J.-M. Bouler, *Drug Discov. Today* 2010, **15**, 547-552.
3. Y. Sun, X.-Y. Chen, Y.-J. Zhu, P.-F. Liu, M.-J. Zhu, Y.-R. Duan, *J. Mater. Chem.* 2012, **22**, 5128-5136.
4. Q.-L. Tang, Y.-J. Zhu, J. Wu, F. Chen, S.-W. Cao, *Nanomedicine: Nanotechnology, Biology and Medicine* 2011, **7**, 428-434.
5. K.-W. Wang, Y.-J. Zhu, X.-Y. Chen, W.-Y. Zhai, Q. Wang, F. Chen, J. Chang, Y.-R. Duan, *Chem. Asian J.* 2010, **5**, 2477-2482.
6. A. Tabaković, M. Kester, J. H. Adair, *Wiley Interdisciplinary Reviews: Nanomedicine and Nanobiotechnology* 2012, **4**, 96-112.
7. K. Baler, J. P. Ball, Z. Cankova, R. A. Hoshi, G. A. Ameer, J. B. Allen, *Biomaterials Science* 2014, **2**, 1355-1366.
8. S. M. Shiels, K. D. Solomon, M. Pilia, M. R. Appleford, J. L. Ong, *Journal of Biomedical Materials Research Part A* 2012, **100A**, 3117-3123.
9. S. Bose, S. Tarafder, *Acta Biomaterialia* 2012, **8**, 1401-1421.
10. J. Zhou, H. Lin, T. Fang, X. Li, W. Dai, T. Uemura, J. Dong, *Biomaterials.* 2010, **31**, 1171-1179.
11. M. Gruselle, T. Kanger, R. Thouvenot, A. Flambard, K. Kriis, V. Mikli, R. Traksmaa, B. Maaten, K. Tõnsuaadu, *ACS Catal.* 2011, **1**, 1729-1733.
12. J. Xu, T. White, P. Li, C. He, Y.-F. Han, *J. Am. Chem. Soc.* 2010, **132**, 13172-13173.

13. L. Li, Y. Liu, J. Tao, M. Zhang, H. Pan, X. Xu, R. Tang, *J. Phys. Chem. C* 2008, **112**, 12219-12224.
14. F. Chen, P. Huang, Y.-J. Zhu, J. Wu, D.-X. Cui, *Biomaterials.* 2012, **33**, 6447-6455.
15. S.-D. Jiang, Q.-Z. Yao, G.-T. Zhou, S.-Q. Fu, *J. Phys. Chem. C* 2012, **116**, 4484-4492.
16. J. Oliva, J. Cama, J. L. Cortina, C. Ayora, J. De Pablo, *J. Hazard. Mater.* 2012, **213–214**, 7-18.
17. M. Jarcho, *Clin. Orthop. Relat. R.* 1981, **157**, 259-278.
18. C. P. A. T. Klein, K. de Groot, A. A. Drissen, H. B. M. van der Lubbe, *Biomaterials.* 1985, **6**, 189-192.
19. S. Kotani, Y. Fujita, T. Kitsugi, T. Nakamura, T. Yamamuro, C. Ohtsuki, T. Kokubo, *J. Biomed. Mater. Res.* 1991, **25**, 1303-1315.
20. Y. B. Kim, G. Kim, *J. Mater. Chem.* 2012, **22**, 16880-16889.
21. C. Weinand, I. Pomerantseva, C. M. Neville, R. Gupta, E. Weinberg, I. Madisch, F. Shapiro, H. Abukawa, M. J. Troulis, J. P. Vacanti, *Bone* 2006, **38**, 555-563.
22. H. Cao, N. Kuboyama, *Bone* 2010, **46**, 386-395.
23. M. G. Yeo, G. H. Kim, *Chem. Mater.* 2011, **24**, 903-913.
24. R. L. Karlinsey, A. C. Mackey, E. R. Walker, K. E. Frederick, *Acta Biomaterialia* 2010, **6**, 969-978.
25. S. Hong, M. Kim, G. Kim, *J. Mater. Chem.* 2012, **22**, 22565-22574.
26. B. H. Fellah, P. Layrolle, *Acta Biomaterialia* 2009, **5**, 735-742.
27. P. Layrolle, A. Lebugle, *Chem. Mater.* 1994, **6**, 1996-2004.
28. J. Chen, Y. Wang, X. Chen, L. Ren, C. Lai, W. He, Q. Zhang, *Mater. Lett.* 2011, **65**, 1923-1926.
29. K. P. Sanosh, M.-C. Chu, A. Balakrishnan, T. N. Kim, S.-J. Cho, *Current Applied Physics* 2010, **10**, 68-71.
30. L. Sha, Y. Liu, Q. Zhang, M. Hu, Y. Jiang, *Mater. Chem. Phys.* 2011, **129**, 1138-1141.
31. J. S. Cho, D. S. Jung, J. M. Han, Y. C. Kang, *Materials Science and Engineering: C* 2009, **29**, 1288-1292.
32. M. Bohner, T. J. Brunner, N. Doebelin, R. Tang, W. J. Stark, *J. Mater. Chem.* 2008, **18**, 4460-4467.
33. J. Tao, H. Pan, H. Zhai, J. Wang, L. Li, J. Wu, W. Jiang, X. Xu, R. Tang, *Cryst.Growth Des.* 2009, **9**, 3154-3160.
34. A. Jillavenkatesa, R. A. Condrate, *Spectrosc. Lett.* 1998, **31**, 1619-1634.
35. L. C. Palmer, C. J. Newcomb, S. R. Kaltz, E. D. Spoerke, S. I. Stupp, *Chem. Rev.* 2008, **108**, 4754-4783.
36. T. Higuchi, *J. Pharm. Sci.* 1963, **52**, 1145-1149.
37 T. Higuchi, *J. Pharm. Sci.* 1961, **50**, 874-875.
38. X.-Y. Zhao, Y.-J. Zhu, F. Chen, B.-Q. Lu, J. Wu, *CrystEngComm* 2013, **15**, 206-212.
39. C. Qi, Y.-J. Zhu, B.-Q. Lu, X.-Y. Zhao, J. Zhao, F. Chen, J. Wu, *Chem. Eur. J.* 2013, **19**, 5332-5341.
40. C. Qi, Y.-J. Zhu, B.-Q. Lu, X.-Y. Zhao, J. Zhao, F. Chen, *J. Mater. Chem.* 2012, **22**, 22642-22650.
41. I. Langmuir, *J. Am. Chem. Soc.* 1916, **38**, 2221-2295.
42. I. Langmuir, *J. Am. Chem. Soc.* 1918, **40**, 1361-1403.
43. H. M. F. Freundlich, *Z.Phys. Chem.* 1906, **57**, 385-470.
44. M. I. Temkin, *Zh. Fiz. Chim* 1941, **15**, 296-332.
45. S. Lagergren, *K. Sven. Vetenskapsakad. Handl.* 1898, **24**, 1-39.
46. Y. S. Ho, G. McKay, *Process. Biochem.* 1999, **34**, 451-465.
47. W. J. Weber, *J. Sanit. Eng. Div. Am. Soc. Civ. Eng.* 1963, **89**, 31-60.
48. K. Henzler, A. Wittemann, E. Breininger, M. Ballauff, S. Rosenfeldt, *Biomacromolecules* 2007, **8**, 3674-3681.
49. Y. Lvov, K. Ariga, I. Ichinose, T. Kunitake, *Thin Solid Films* 1996, **284–285**, 797-801.